

Characterisation and performance of the PADME electromagnetic calorimeter

To cite this article: P. Albicocco *et al* 2020 *JINST* **15** T10003

View the [article online](#) for updates and enhancements.



IOP | ebooks™

Bringing together innovative digital publishing with leading authors from the global scientific community.

Start exploring the collection—download the first chapter of every title for free.

TECHNICAL REPORT

Characterisation and performance of the PADME electromagnetic calorimeter

The PADME collaboration

P. Albicocco,^a J. Alexander,^b F. Bossi,^a P. Branchini,^c B. Buonomo,^a C. Capoccia,^a E. Capitulo,^a G. Chiodini,^d A.P. Caricato,^{d,e} R. de Sangro,^a C. Di Giulio,^a D. Domenici,^a F. Ferrarotto,^f G. Finocchiaro,^a S. Fiore,^{f,g} L.G. Foggetta,^a A. Frankenthal,^b G. Georgiev,^{h,a} A. Ghigo,^a F. Giacchino,^a P. Gianotti,^a S. Ivanov,^h V. Kozhuharov,^{h,a} E. Leonardi,^f B. Liberti,ⁱ E. Long,^{j,f} M. Martino,^{d,e} I. Oceano,^{d,e} F. Oliva,^{d,e} G.C. Organtini,^{j,f} G. Piperno,^{f,j,1} M. Raggi,^{j,f} F. Safai Tehrani,^f I. Sarra,^a B. Sciascia,^a R. Simeonov,^h A. Saputi,^a T. Spadaro,^a S. Spagnolo,^{d,e} E. Spiriti,^a D. Tagnani,^c C. Taruggi,^{a,k} L. Tsankov,^h P. Valente^f and E. Vilucchi^a

^aINFN Laboratori Nazionali di Frascati,
Via E. Fermi 54, 00044 Frascati, Italy

^bDepartment of Physics, Cornell University,
109 Clark Hall, Ithaca, NY 14853, U.S.A.

^cINFN Sezione di Roma 3,
Via della Vasca Navale, 84, 00146 Roma RM, Italy

^dINFN Sezione di Lecce,
Via Provinciale per Arnesano, 73100 Lecce, Italy

^eDipartimento di Matematica e Fisica, Università del Salento,
Via Provinciale per Arnesano, 73100 Lecce, Italy

^fINFN Sezione di Roma,
p.le Aldo Moro 5, 00185 Roma, Italy

^gENEA centro ricerche Frascati,
Via Enrico Fermi 45, 00044 Frascati (Roma), Italy

^hUniversity of Sofia St. Kl. Ohridski,
15 Tsar Osvoboditel Blvd, 1504 Sofia, Bulgaria

ⁱINFN Sezione di Roma Tor Vergata,
Via della Ricerca Scientifica 1, 00133 Roma, Italy

^jDipartimento di Fisica, Sapienza Università di Roma,
P.le Aldo Moro 5, 00185 Roma, Italy

^kDipartimento di Fisica Università di Roma Tor Vergata,
Via della Ricerca Scientifica 1, 00133 Roma, Italy

E-mail: gabriele.piperno@roma1.infn.it

¹Corresponding author.

ABSTRACT: The PADME experiment at the LNF Beam Test Facility searches for dark photons produced in the annihilation of positrons with the electrons of a fixed target. The strategy is to look for the reaction $e^+ + e^- \rightarrow \gamma + A'$, where A' is the dark photon, which cannot be observed directly or via its decay products. The electromagnetic calorimeter plays a key role in the experiment by measuring the energy and position of the final-state γ . The missing four-momentum carried away by the A' can be evaluated from this information and the particle mass inferred. This paper presents the design, construction, and calibration of the PADME's electromagnetic calorimeter. The results achieved in terms of equalisation, detection efficiency and energy resolution during the first phase of the experiment demonstrate the effectiveness of the various tools used to improve the calorimeter performance with respect to earlier prototypes.

KEYWORDS: Calorimeters; Detector design and construction technologies and materials; Gamma detectors (scintillators, CZT, HPGe, HgI etc)

ARXIV EPRINT: [2007.14240](https://arxiv.org/abs/2007.14240)

Contents

| | | |
|----------|---|-----------|
| 1 | Introduction | 1 |
| 2 | The PADME experiment | 2 |
| 3 | The PADME electromagnetic calorimeter | 2 |
| 3.1 | Detector characteristics | 2 |
| 3.2 | Scintillating units production | 4 |
| 3.3 | Signal readout and trigger | 4 |
| 4 | Scintillating units calibration and equalisation | 5 |
| 4.1 | Pre-assembly calibration with ^{22}Na | 5 |
| 4.2 | Cosmic rays | 7 |
| 4.3 | Calorimeter performance with positron beam | 10 |
| 5 | Conclusions | 12 |

1 Introduction

A possible explanation for the elusiveness of dark matter (DM) is that it interacts with standard model (SM) particles only by means of a mediator that feebly couples to them. One of the simplest theoretical models based on this assumption introduces a new U(1) gauge symmetry with a vector boson mediator, the dark photon (DP), or A' [1, 2]. SM particles are neutral under this new symmetry but the A' could faintly interact with them because of a kinetic mixing with the ordinary photon. The strength of this interaction is given by an effective charge εq , where q is the electric charge of the particle and ε is the kinetic mixing coefficient.

The Positron Annihilation into Dark Matter Experiment (PADME), ongoing at the Laboratori Nazionali di Frascati (LNF) of the Istituto Nazionale di Fisica Nucleare (INFN), aims to explore this theoretical scenario. For this purpose, a dedicated detector was built, whose central component is an electromagnetic calorimeter made of crystals of bismuth germanium oxide (BGO). The calorimeter has high granularity and excellent detection efficiency for photons with energy between 100 and 500 MeV. Sensitivity to the coupling constant down to $1 \cdot 10^{-3}$ could be reached for values of $m_{A'} \leq 23.7 \text{ MeV}/c^2$ collecting 10^{13} positron on target. In the following sections, a short description of the experimental technique is given (section 2), followed by a detailed description of the design solutions adopted for the calorimeter (section 3), and finally a report of the performance reached in terms of efficiency and energy resolution in the 2018-19 PADME commissioning run (section 4).

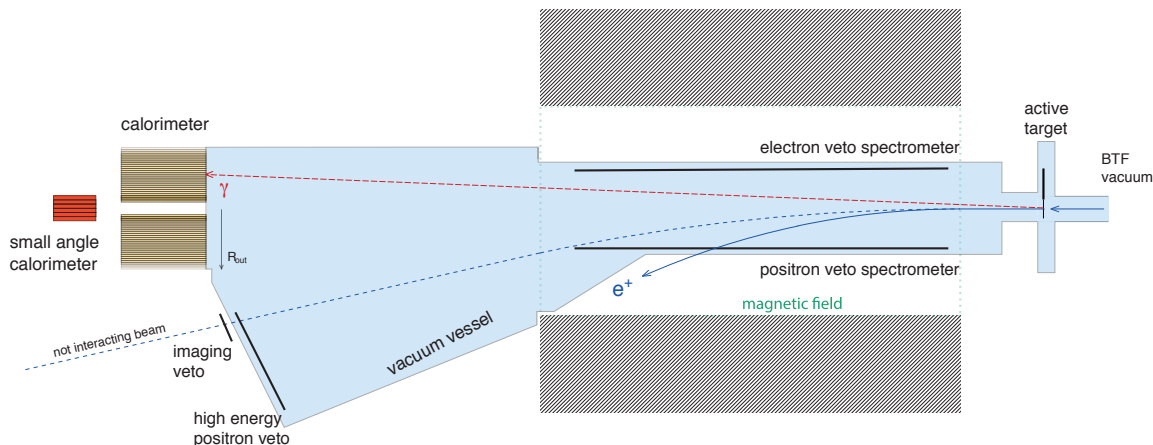


Figure 1. Top view of the PADME detector (not to scale). From right to left: active target, dipole magnet (with e^+/e^- vetoes inside), high-energy positron veto and the calorimeters.

2 The PADME experiment

PADME is hosted at the Beam Test Facility of LNF [3, 4]. It looks for a DP produced via the reaction $e^+ + e^- \rightarrow \gamma + A'$ using positrons accelerated to 550 MeV by the laboratory's LINAC, impinging on the electrons of a 100 μm thick active diamond target, able to measure beam position and intensity [5].

The experimental technique relies on the measurement of the missing mass of the final states with a single photon. By measuring its energy and the direction of flight with a granular electromagnetic calorimeter (ECal), it is possible to measure $m_{A'}^2$, as the square of the missing mass.

In addition to the ECal, the setup consists of a dipole magnet to deflect the beam away from the calorimeter, a charged particle veto system (made of a positron veto, electron veto and high-energy positron veto [6, 7]) to identify positrons that lose part of their energy through Bremsstrahlung, and a fast small angle calorimeter (SAC) [8] to detect and veto Bremsstrahlung photons in the forward direction. A schematic drawing of the detector is shown in figure 1.

A more detailed description of the PADME detector can be found in [9].

3 The PADME electromagnetic calorimeter

The segmented PADME electromagnetic calorimeter was built by reshaping BGO crystals recovered from the endcaps of the calorimeter of the L3 experiment [10]. The following sub-sections present a general description of the calorimeter, the production procedure of the scintillating units (SUs) (i.e. the assembly of a crystal and its photomultiplier tube (PMT)), the solution adopted for the signal digitisation, and finally the trigger systems used to collect data.

3.1 Detector characteristics

ECal consists of 616 BGO crystals ($2.1 \times 2.1 \times 23.0 \text{ cm}^3$) arranged in a cylindrical shape ($\approx 29 \text{ cm}$ external radius) and features a central square hole (5×5 crystals) behind which the SAC is placed.

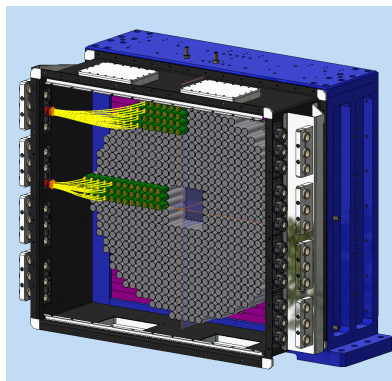


Figure 2. Rear view of the ECal without back closing panel. The blue structure is the mechanical support, and the black case is the cover of the PMTs and their cables, which are shown only for few units. The purple components are plastic fillers (see text for more detail).

The size of the calorimeter is a compromise between large acceptance, good angular resolution, and the space available in the experimental hall. The distance between the target and the ECal is 3.46 m, determining an angular coverage of $[15.7, 82.1]$ mrad. For the SAC, the covered region is $[0, 18.9]$ mrad. The numbers in brackets report respectively half of the minimum and of the maximum opening angle of a cone with vertex at the target and base contained by the front face of the corresponding calorimeter.

The main requirements for the ECal crystals are a small Molière radius, and an energy resolution of roughly $2\%/\sqrt{E}$. BGO was chosen because it satisfies these conditions and because BGO crystals were available for reuse from the L3 experiment [10].

The crystal transverse dimensions were chosen to provide excellent position resolutions, while the longitudinal dimensions of the crystals, slightly more than 20 radiation lengths, were imposed by the original L3 crystal length.

The central square hole allows the passage of forward emitted Bremsstrahlung photons, detected by the SAC. The high rate of these photons would flood the inner ECal crystals. On the contrary, being based on Cherenkov radiator (PbF_2), the SAC is able to sustain particle rates up to hundreds of MHz, thanks to a signal length of only 3 ns, much shorter with respect to BGO scintillation light decay time of ~ 300 ns [11].

A CAD drawing of the calorimeter is presented in figure 2. The metallic support structure has a square shape chosen to ease the detector assembly. The remaining free space between the frame and the crystals is filled with plastic elements. This also puts BGO in contact with a low-density material instead of metal where photons could produce showers with higher probability. All HV and signal cables exit from the back in groups of 64, passing through two holders, the inner one light-tight.

Due to the low energy of the photons in PADME, any single crystal support structure could spoil the energy resolution by introducing dead materials. In assembling the calorimeter special care has been taken to control size differences among the SUs which were individually selected on the basis of their dimensions. $50\ \mu\text{m}$ black Tedlar[®] [12] strips were used to compensate for differences in their heights. To reduce light cross-talk, additional Tedlar[®] strips were inserted vertically between adjacent crystals, while foils were placed horizontally between consecutive layers.

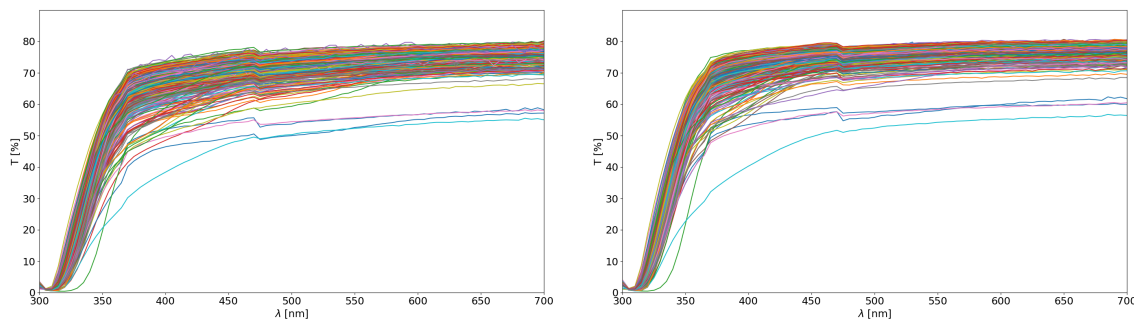


Figure 3. BGO transparency as a function of wavelength, before (left) and after (right) annealing. The improvement is visible especially at lower wavelengths.

3.2 Scintillating units production

The process of building scintillating units for the ECal required different steps. First, the old reflective paint and photodiodes were removed from the original L3 crystals. To recover performance deterioration due to radiation damage, crystals underwent accelerated annealing at CERN’s LAB 27:

1. crystals were heated from room temperature to 200 °C over 3 h;
2. they were kept at 200 °C for 6 h;
3. finally, they were cooled down from 200 °C back to room temperature over about 1 day.

Figure 3 shows measurements of the transparency before (left) and after (right) annealing. The improvement in transparency at lower wavelengths is clearly visible.

Since the original shape of the crystals was tapered pyramidal, they were cut at Gestione SILO (Italy) [13] to have rectangular faces. The same firm also glued the PMTs (using the ELJEN EJ-500 optical cement [14]) and coated the BGO with three layers ($\approx 60 \mu\text{m}$) of ELJEN EJ-510 (a bright white diffusive paint with titanium dioxide pigments [15]).

The PMTs used in the experiment are the HZC XP1911 type B [16], with a quantum efficiency of 21% at 480 nm (the BGO maximum emittance wavelength) and a 19 mm diameter. The gain curve of each PMT was studied before gluing by flashing a blue LED in front of the photocathode using different PMT HV values, and measuring the corresponding charge collected by each tube.

3.3 Signal readout and trigger

ECal PMT signals are digitised using CAEN V1742 boards [17, 18]. These host 4 DRS4 ASICs (a switched-capacitor array sampling chip) and provide a total of 32 channels. Each channel has a dynamic range of 1 V with 12-bit precision.

The board has selectable sampling frequency (1 GS/s, 2.5 GS/s, or 5 GS/s) and a memory depth of 1024 samples/channel. The selected sampling frequency for ECal signals is 1 GS/s, to obtain a 1 μs long digitisation window able to match the long decay time of BGO scintillation light. Figure 4 illustrates a typical calorimeter pulse.

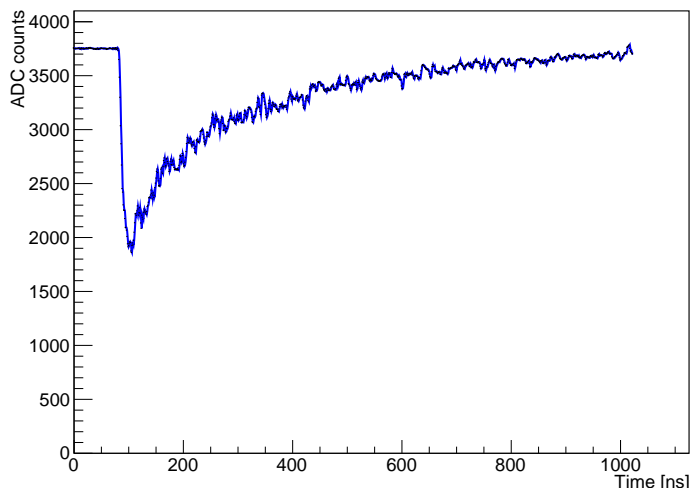


Figure 4. A typical ECal signal digitized with a sampling frequency of 1 GS/s.

For each digitisation window, some samples before the BGO signal leading edge are collected to evaluate the pulse base-line, which is obtained as the mean of the first 50 pre-pulse samples. The total collected charge is then calculated summing over all the acquired samples and subtracting the base-line value. Algorithms to correct for possible cuts on the pulse tail and for variation of the particle energy loss are also implemented.

During the data-taking two different kind of triggers are used, calibration trigger and physics trigger:

1. Cosmic ray (CR) trigger: provided by two scintillating slabs, placed above and below the ECal (see section 4.2). Its purpose is to check the SUs stability using signals from minimum ionizing particles (MIPs);
2. Beam trigger: generated by the accelerator complex for each bunch, and used in data-taking for physics.

4 Scintillating units calibration and equalisation

SUs were calibrated with a ^{22}Na source before mounting in the calorimeter. This was done to determine the charge vs HV curve used to set the SU voltage to the desired gain. After the installation of ECal in the experimental hall, the CR trigger was also used to check the response of the units to MIPs. Using CR events, it is possible to validate the ^{22}Na calibration and to assess and improve the SUs equalisation.

4.1 Pre-assembly calibration with ^{22}Na

To select and equalise the response of each SU, a dedicated setup was built exploiting the two back-to-back 511 keV photons emitted by a ^{22}Na source. It allows the scan of a 5×5 SU matrix with the source moving in front of each crystal. Figure 5 (left) shows a drawing with the sodium path highlighted and figure 5 (right) shows a photograph of the test stand. A $3 \times 3 \times 20 \text{ mm}^3$

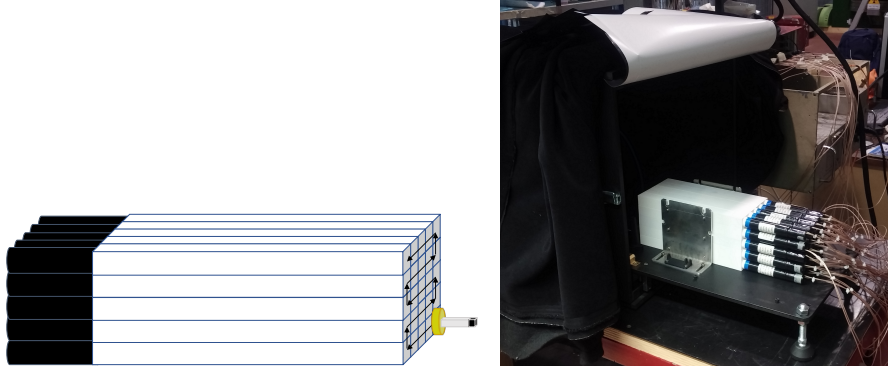


Figure 5. Setup for SUs calibration. Left: sketch of the test stand (not to scale), with the ^{22}Na source indicated with a yellow disk (possible motions are also shown). A LYSO crystal is placed on the opposite side of the source to provide the trigger signal. Right: a photograph of the test stand, with a stack of SUs.

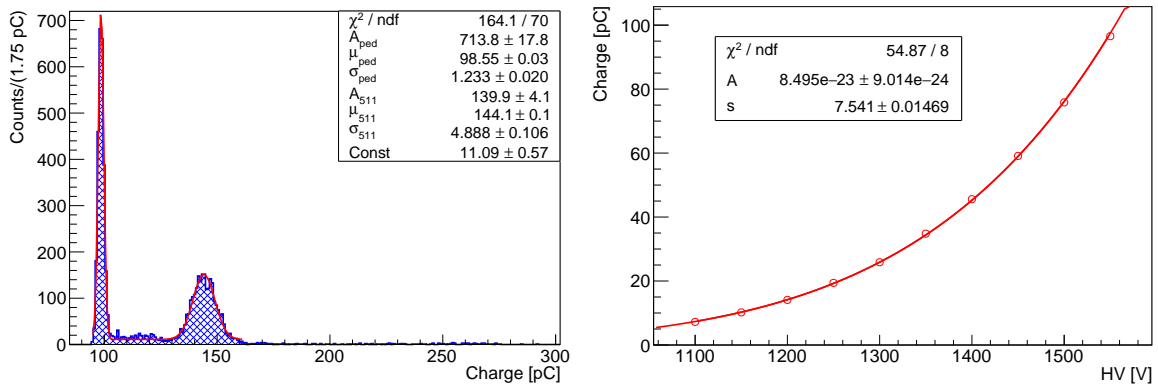


Figure 6. Left: charge distribution of a SU at 1400 V fit with a double Gaussian plus a flat function to reproduce the pedestal, the 511 keV peak, and the constant background. Right: measured charge as a function of HV with the gain curve fit $Q = A \cdot V^s$ superimposed.

LYSO crystal, read out by a SiPM, is placed on the opposite side of the source with respect to the BGO and produces the trigger signal. Data were collected at 10 different voltages in the interval [1100, 1550] V in steps of 50 V, acquiring about 6000 events per HV value.

An example of the charge distribution obtained for a unit at 1400 V is presented in figure 6 (left). The pedestal and the 511 keV signal are clearly visible and both are fitted with a Gaussian, while the approximately flat continuum is modelled with a constant function.

The collected charge, for each value of the HV, was determined as the difference between the 511 keV peak and pedestal position. Figure 6 (right) presents the charge vs HV behaviour with the best-fit curve superimposed (same SU of figure 6 (left)). The fitting curve has the form $Q = A \cdot V^s$, where Q is charge, V is voltage, and A and s are free parameters.

In figure 7, the distribution of voltages needed to obtain a gain of 15.3 pC/MeV is displayed for all 616 PADME SUs. The distribution mean is 1186 V with a standard deviation of 53 V. Even the largest value, 1411 V, is well below the safety operational maximum of 1700 V [16].

To evaluate the reproducibility of calibrations, 135 SUs (22% of the total) underwent a second, identical, measurement campaign. The relative difference between the two optimal HVs, given

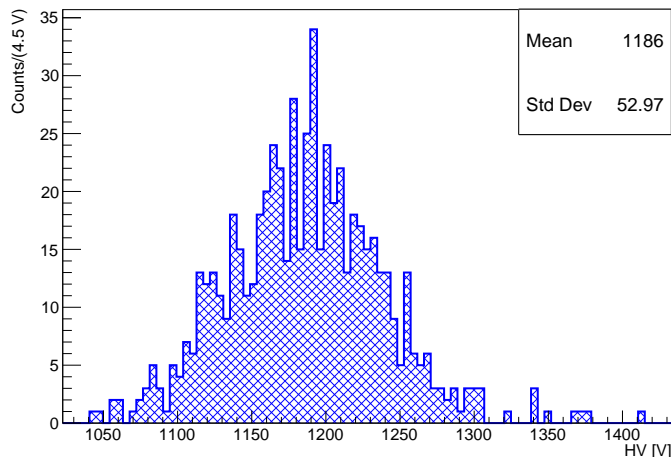


Figure 7. Distribution of PMT voltages used to set the gain of the corresponding SU to 15.3 pC/MeV.

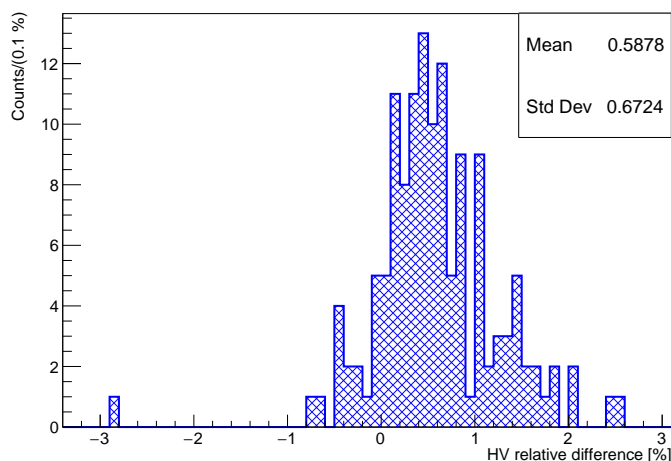


Figure 8. Relative difference between voltage measurements for the 135 SUs that were tested a second time to assess gain curve reproducibility. The required gain is 15.3 pC/MeV in both cases.

by $\frac{V_1 - V_2}{(V_1 + V_2)/2}$, remains below a few percent as shown in figure 8. This difference also incorporates possible temperature variations between the two measurements.

4.2 Cosmic rays

Since the start of data-taking, the calorimeter has been operated with voltages corresponding to a gain of 15.3 pC/MeV. As shown in figure 9, the calorimeter is equipped with a CR trigger, made by two plastic scintillator slabs, one above and one below the ECal, and each read out by two PMTs (one per side). The trigger logic implemented is also detailed in the figure.

Figure 10 gives an example of a cosmic ray passing through the entire calorimeter. The numbers in the various positions indicate the charge collected by each SU, in pC.

The calorimeter equalisation is checked by studying the charge distributions obtained from cosmic rays in the various SUs. For a more precise evaluation, only cosmics crossing crystals

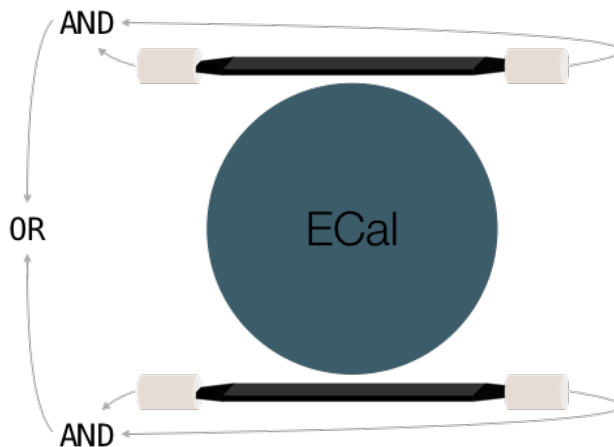


Figure 9. Structure and logic of the ECal CR trigger. It consists of two plastic scintillator slabs, one above and one below the ECal. Each bar is read out by two PMTs, one per side, set in logic AND. The logic OR of the two ANDs gives the trigger signal.

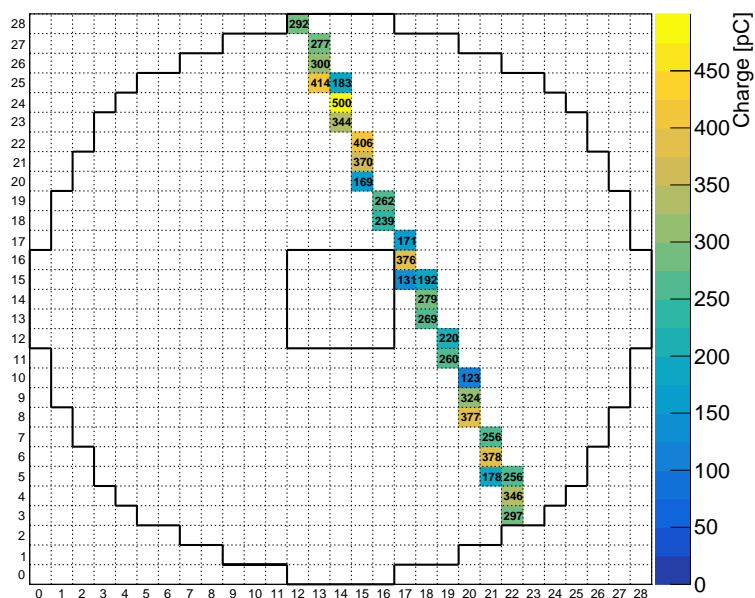


Figure 10. A cosmic ray passing through the ECal. The color scale and numbers inside the squares represent the charge collected by the SU.

vertically are considered. This is defined by three conditions:

- a cosmic ray passes through three SUs aligned in a column;
- there are no other signals in the three rows of the SUs under consideration;
- only the pulse from the central SU is considered for the calculation.

This ensures that the cosmic ray releases little energy in adjacent crystals. For example, in figure 10, only SUs in position (15,21) and (20,9) satisfy these requirements. For peripheral units without any SUs directly above or below (68, corresponding to 11% of the total), the two crystals below or above are used, respectively.

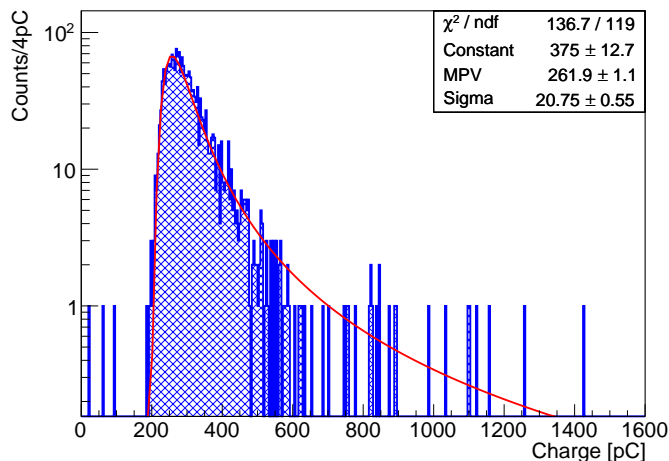


Figure 11. Example of charge distribution given by CRs passing vertically through a SU. A Landau fit is superimposed.

An example of the charge distribution produced by this selection, with a superimposed Landau fit, is given in figure 11. Landau parameters are those defined by the ROOT package [19] and the algorithm is from CERNLIB G110 DENLAN, which is based on [20].

Figure 12 presents the most probable values (MPVs) from Landau fits performed on charge distributions obtained from CR data collected over three days. On the left, the 2D distribution (with values and color scale) is shown and on the right two histograms are superimposed: the blue histogram corresponds to all active SUs while the red one excludes the 68 peripheral units. The means of the two Gaussian fits are compatible: (266.3 ± 1.4) pC and (266.0 ± 1.4) pC, respectively. Taking into account the Gaussian for all the units, the ECal equalisation achieved using the gain curves from the ^{22}Na source indicates a signal spread of $(10.99 \pm 0.48)\%$, where the spread is expressed as the ratio of the sigma and of the mean of the Gaussian fit.

Empty squares on the left plot of figure 12 indicate 4 non-operational channels. If one of these belongs to the triplet needed to define the verticality condition, it is skipped and the one above or below is used. This study also helps to improve the calorimeter energy resolution. Assuming that, on average, CRs release the same amount of energy in all crystals, the MPV of each charge distribution can be used as a normalisation term, by simply dividing each pulse integral by the MPV of the corresponding ECal channel.

Finally, CRs are also used to evaluate the SU efficiency. With the same triplets defined in the previous analysis, the efficiency of the central SU can be determined. The efficiency is defined as the ratio between the number of events with hits in all three cells and that with hits only in the two external ones. Figure 13 (left) shows the 2D distribution of ECal efficiencies. They have been evaluated using a CR data set taken over three days. Figure 13 (right) reports the measured efficiencies with a zoom on the interval $[97, 101]\%$ in the inset. A reverse Landau fit is superimposed on both distributions.

Figure 14 reports the cumulative efficiency distribution of SUs. The percentage is given without considering the 4 non-operational units and the 68 edge SUs.

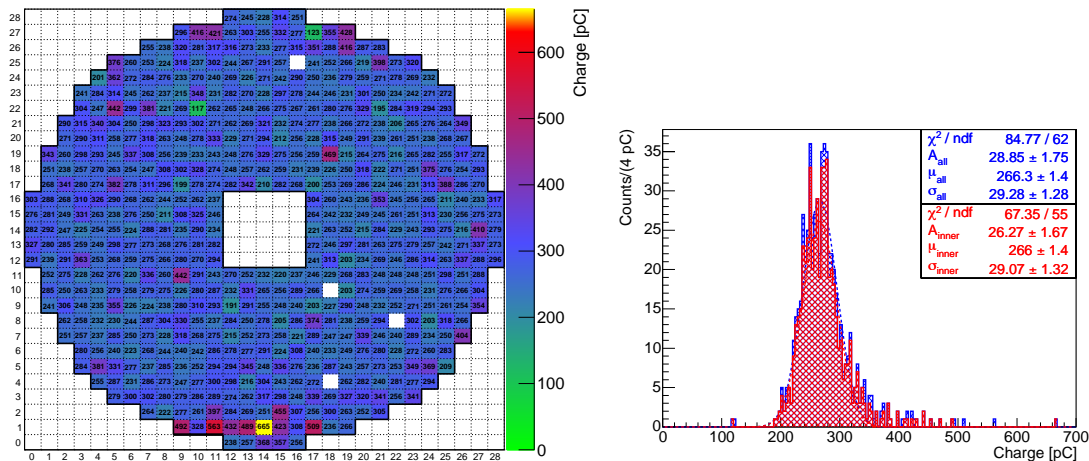


Figure 12. MPVs obtained from Landau fits to the charge distributions produced by CRs passing vertically through SUs. Left: map of charge measurement in the ECal. The 4 white squares correspond to non-operational SUs. Right: MPV distributions considering (blue) and not considering (red) the 68 edge crystals.

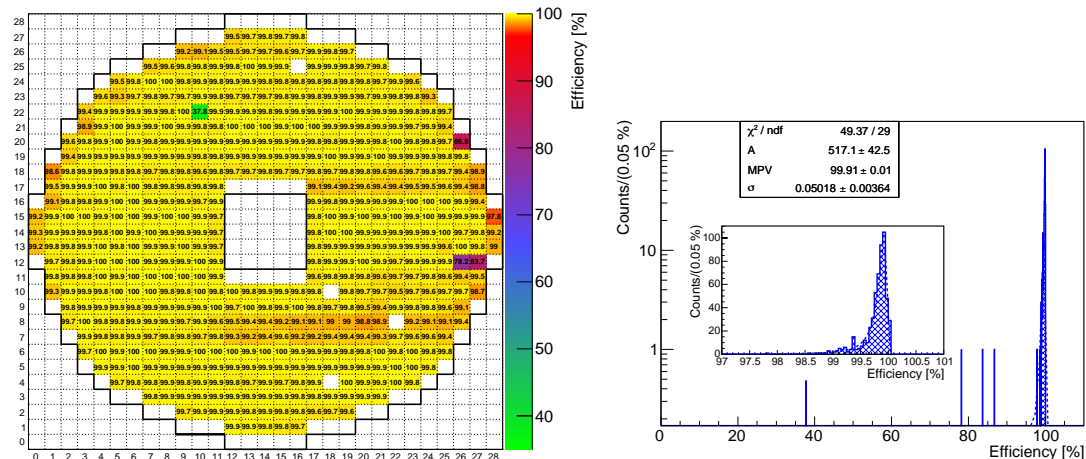


Figure 13. Efficiency of SUs, evaluated using CR data. Left: ECal efficiency map. Right: efficiency distribution with a reversed Landau fit superimposed (see text). In the inset, a zoom on the region [97, 101]%. Both plots exclude the 4 non-operational units and the 68 edge units.

4.3 Calorimeter performance with positron beam

Before ECal construction, several tests were performed on a prototype consisting in a 5×5 matrix of BGO crystals ($2.0 \times 2.0 \times 22.0 \text{ cm}^3$) read out by XP1912 HZC PMTs. In particular, single-positron beams of different energies were fired at the central crystal of the matrix. These measurements reveal an energy resolution compatible with the desired performance [21]:

$$\frac{\sigma(E)}{E} = \frac{2.0\%}{\sqrt{E[\text{GeV}]}} \oplus \frac{0.003\%}{E[\text{GeV}]} \oplus 1.1\%.$$

Figure 15 presents the energy resolution measured during these tests. Blue (red) squares identify results obtained with a 250 MeV (450 MeV) beam energy. During the same test the charge response as a function of the deposited energy has been shown to be linear in within 2% up to 1 GeV.

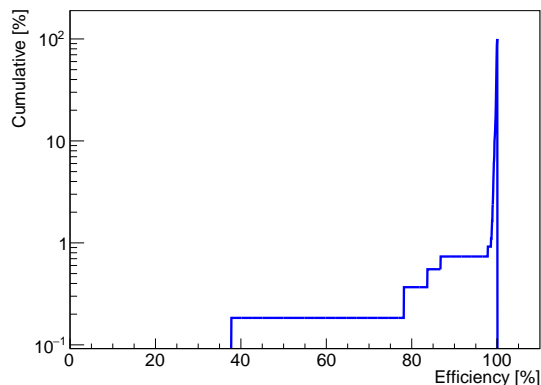


Figure 14. Cumulative efficiency distribution of figure 13, in percent. The percentage is given without considering the 4 non-operational units and the 68 edge units.

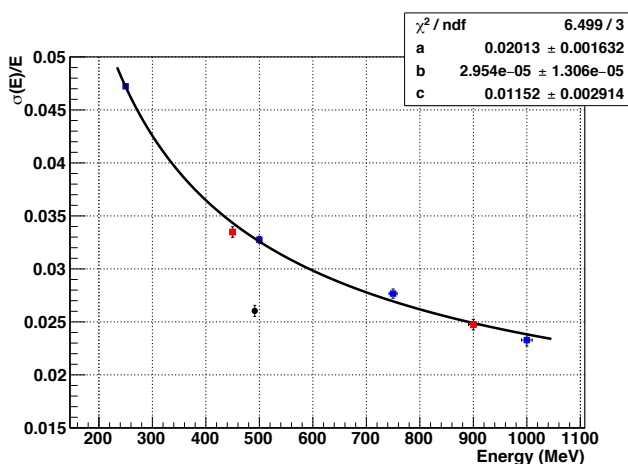


Figure 15. Energy resolution measured with the ECal prototype (red and blue points) [21] compared with the ECal result on special run data set (black point).

To evaluate the energy resolution of ECal a special run was performed with a 490 MeV positron beam energy (multiplicity ≈ 1) fired directly at the calorimeter. A 5×5 cluster, around the crystal with the largest energy deposit, was considered to simulate the prototype condition (other clusterization algorithms implemented by the PADME collaboration are discussed in [22]). The measured energy resolution turned out to be 2.62 ± 0.05 (stat)%, as shown by the black circle in figure 15. This improvement was partially expected since the prototype detector was slightly different from the final calorimeter. Several factors contributed to improve the performance of the ECal with respect to the prototype:

- The ECal has longer crystals and therefore a better energy containment;
- PMTs are glued to the BGO while in the prototype they were optically coupled with optical grease;
- ECal crystals are painted and not simply wrapped with PTFE tape;
- The ECal SUs responses are equalised a priori while at the test beam all SUs were operated at the same voltage of 1100 V.

The beam characteristics also contributes to the measured energy resolution: the beam used for the prototype test was not optimised as in the standard data-taking. In fact, in order to be able to change its energy, electrons produced on a secondary target were used. This was necessary since the main user of the LINAC primary beam was the DAΦNE LNF collider requiring a fixed energy (550 MeV). A primary beam, 10^9 particles/bunch, was hitting a secondary target and electrons of desired energy, produced by the electromagnetic showers, were then selected with a dipole magnet. Due to the high multiplicity, the showers also produced many photons that could reach the prototype under test, inducing background. Conversely, in the ECal test, the beam was a primary beam consisting only of 490 MeV positrons. In this case the LINAC gun was off and only few electrons were accelerated, the ones produced by the gun's dark current in phase with the accelerating field. This very low multiplicity helped reducing the beam-induced photon background reaching the ECal improving the measured energy resolution.

5 Conclusions

The primary goal of the PADME experiment is to measure with high efficiency and precision the SM photons produced by the reaction $e^+ + e^- \rightarrow \gamma + A'$, where the dark photon A' signal appears as missing mass. This is obtained by means of an electromagnetic calorimeter made of 616 BGO crystals.

Each SU was calibrated with a ^{22}Na source before installation in order to set the working point to 15.3 pC/MeV. Owing to the implementation of a cosmic ray trigger, the calibration of SUs was continuously monitored during physics data-taking. The same system also allowed SUs equalisation and efficiency evaluation. The measured gain spread is $(10.99 \pm 0.48)\%$, while the efficiency is $\geq 98\%$ for 99.1% of the channels.

Finally, to check the energy resolution, a dedicated measurement was performed by firing a single positron beam of 490 MeV energy at the calorimeter. The obtained resolution is 2.62 ± 0.05 (stat)%, with an evident improvement compared to the values obtained with a calorimeter prototype.

Acknowledgments

The PADME collaboration wants to warmly thank the BTF and LINAC teams, for the excellent quality of the beam provided during the test run. The PADME collaboration wants to thanks the technical staff of LNF for the work done. Among the others a special mention goes to R. Lenci, and G. Papalino for their help in assembling and cabling the detector.

University of Sofia group is partially supported under BG-NSF DN08-14/14.12.2016 and the MoU SU — LNF-INFN 70-06-497/07-10-2014.

References

- [1] P. Galison and A. Manohar, *Two Z's or not two Z's?*, *Phys. Lett. B* **136** (1984) 279.
- [2] B. Holdom, *Two U(1)'s and ϵ charge shifts*, *Phys. Lett. B* **166** (1986) 196.
- [3] A. Ghigo, G. Mazzitelli, F. Sannibale, P. Valente and G. Vignola, *Commissioning of the DAΦNE beam test facility*, *Nucl. Instrum. Meth. A* **515** (2003) 524.
- [4] P. Valente et al., *Linear Accelerator Test Facility at LNF: Conceptual Design Report*, [arXiv:1603.05651](https://arxiv.org/abs/1603.05651).
- [5] R. Assiro et al., *Performance of the diamond active target prototype for the PADME experiment at the DAΦNE BTF*, *Nucl. Instrum. Meth. A* **898** (2018) 105 [[arXiv:1709.07081](https://arxiv.org/abs/1709.07081)].
- [6] F. Ferrarotto et al., *Performance of the Prototype of the Charged-Particle Veto System of the PADME Experiment*, *IEEE Trans. Nucl. Sci.* **65** (2018) 2029.
- [7] S. Ivanov and K. Venelin, *The charged particle veto system of the PADME experiment*, *AIP Conf. Proc.* **2075** (2019) 080005.
- [8] A. Frankenthal et al., *Characterization and performance of PADME's Cherenkov-based small-angle calorimeter*, *Nucl. Instrum. Meth. A* **919** (2019) 89 [[arXiv:1809.10840](https://arxiv.org/abs/1809.10840)].
- [9] M. Raggi and V. Kozhuharov, *Proposal to Search for a Dark Photon in Positron on Target Collisions at DAΦNE Linac*, *Adv. High Energy Phys.* **2014** (2014) 959802 [[arXiv:1403.3041](https://arxiv.org/abs/1403.3041)].
- [10] L3 collaboration, *The Construction of the L3 Experiment*, *Nucl. Instrum. Meth. A* **289** (1990) 35.
- [11] PARTICLE DATA GROUP collaboration, *Review of Particle Physics*, *Prog. Theor. Exp. Phys.* **2020** (2020) 083C01.
- [12] https://www.dupont.com/content/dam/dupont/amer/us/en/photovoltaic/public/documents/DEC_Tedlar_GeneralProperties.pdf.
- [13] <https://www.gestionesilo.it/>.
- [14] <http://www.ggg-tech.co.jp/maker/eljen/ej-500.html>.
- [15] <http://www.ggg-tech.co.jp/maker/eljen/ej-510.html>.
- [16] http://www.hzcphotonics.com/en_introduction%20of%20products.html.
- [17] <https://www.caen.it/products/v1742/>.
- [18] E. Leonardi et al., *Development and test of a DRS4-based DAQ system for the PADME experiment at the DAΦNE BTF*, *J. Phys. Conf. Ser.* **898** (2017) 032024.
- [19] *ROOT Data Analysis Framework*, <https://root.cern.ch/>.
- [20] K.S. Kolbig and B. Schorr, *A Program Package for the Landau Distribution*, *Comput. Phys. Commun.* **31** (1984) 97 [*Erratum ibid.* **178** (2008) 972].
- [21] M. Raggi et al., *Performance of the PADME Calorimeter prototype at the DAΦNE BTF*, *Nucl. Instrum. Meth. A* **862** (2017) 31.
- [22] E. Leonardi, G. Piperno and M. Raggi, *Evaluation of clustering algorithms at the < 1 GeV energy scale for the electromagnetic calorimeter of the PADME experiment*, *J. Phys. Conf. Ser.* **898** (2017) 072019.